

A low-temperature high-sensitivity torsion balance magnetometer with *in situ* stator adjustment

A J Matthews, A Usher and C D H Williams

*Quantum Interacting Systems Group, School of Physics, University of Exeter,
Stocker Road, Exeter, Devon, United Kingdom, EX4 4QL*

Abstract

Torsion balance magnetometry can be used as a versatile probe of two-dimensional electron systems. We have developed a highly sensitive magnetometer, utilising capacitive proximity detection of the rotor position, for use at temperatures below 10 mK. The instrument incorporates two piezo-electric linear motors to enable the stator positions to be adjusted *in situ* at base temperature. The magnetometer responsivity is inversely proportional to the square of the rotor–stator separation and the novel linear motor technique, accompanied by effective vibration isolation and optimised capacitance bridge electronics, achieves a resolution $6.5 \times 10^{-12} \text{ N m Hz}^{-1/2}$.

Introduction

Magnetisation measurements have been used to study two-dimensional electron systems (2DESs) for many years. They provide information about the equilibrium magnetisation (de Haas – van Alphen (dHvA) effect) [1-8], which can probe the density of states of the 2DES. Also, non-equilibrium eddy currents (ECs) induced by sweeping the applied magnetic field when the sample is in the low-dissipation states of the integer and fractional quantum Hall effect (IQHE and FQHE) regimes, can be used for contact-free transport measurements [9-11]. However, to observe these effects, extreme experimental conditions – high magnetic fields and low temperatures – are required and the magnetometer must be very sensitive. Both cantilever [5,6] and torsion balance [1,2,3] magnetometers have the sensitivity necessary for measuring the small dHvA signal.

In 2DESs the magnetisation, \mathbf{M} , is constrained to be parallel to the normal to the 2DES plane. Applying a homogeneous magnetic field, \mathbf{B} , at an angle to \mathbf{M} causes a torque,

$$\underline{\tau} = \mathbf{M} \times \mathbf{B}, \quad \{1\}$$

to act on the sample. In our measurements the angle between the normal and the applied field is typically chosen to be around 20° .

The torque can be detected either capacitively [1,2] or optically [6,7] by measuring either a rotation of the magnetometer [1,7] (in some cases a feedback technique is employed to reduce the rotor rotation) or a shift in the resonant frequency of torsional oscillations [6,12].

Magnetometer design

We have followed Templeton [2] and developed a ‘differential capacitor’ magnetometer in which the rotor is supported on a torsion fibre above two fixed plates (stators). The rotor is 12 mm square and the stators are both 10×5 mm. The overlap allows for the inclusion of a grounded guard-ring electrode to ensure that there is no capacitive coupling of the stators to the 2DES. A rotation of the rotor results in a change in capacitance of each side of the magnetometer, depicted in figure 1, and this change is detected using an electronic bridge circuit incorporating a virtual-earth transimpedance amplifier. The bridge, which operates at around 10 kHz, will be described in more detail in a later section.

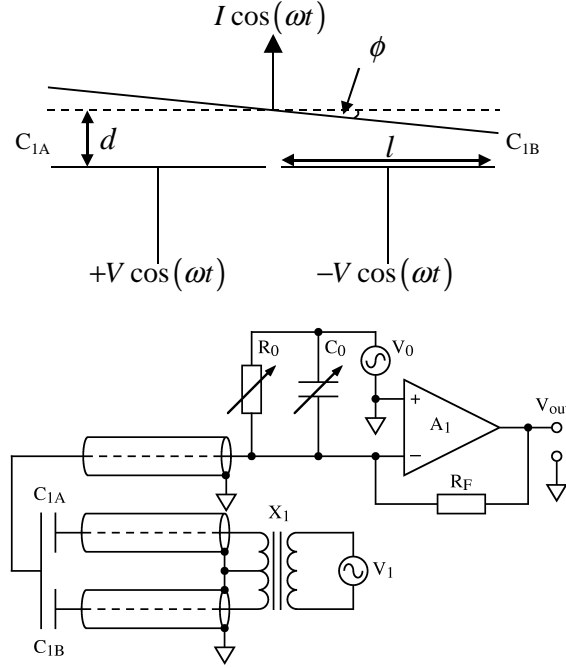


Figure 1. Top, a schematic representation of the differential-capacitor torsion-balance magnetometer. The rotor and stators form a differential capacitor which is part of the detection electronics. Bottom, a simplified schematic diagram of the current-balance bridge circuit. The two voltage sources are derived from the same oscillator.

From figure 1 it can be seen that if the two sides of the differential capacitor have equal capacitances then the current flowing to the virtual earth will be zero. A deflection of the rotor through an angle ϕ will change the capacitance of each side of the magnetometer by $\pm\Delta C$. The new capacitance is,

$$C(\phi) = C_0 \pm \Delta C$$

$$\approx \frac{\epsilon w l}{d} \left[1 \pm \frac{l\phi}{2d} \right]. \quad \{2\}$$

Here ϵ is the permittivity, w is the width of the capacitor plate and the other quantities are as defined in the figure. The measured signal, S , at the output of the bridge is proportional to $2\Delta C$ and hence

$$S \propto \frac{\epsilon w l^2}{d^2} \phi. \quad \{3\}$$

Since we desire the most sensitive instrument possible we wish to maximise the angle responsivity, $G_\phi = \frac{dS}{d\phi}$, of the system (strictly speaking, we wish to achieve the

best *resolution* possible, a quantity that depends on the responsivity, noise level and measurement bandwidth, and which will be defined in a later section). However, ε is a physical constant and neither w nor l can be increased due to the bore size of the superconducting solenoid which provides the magnetic field for the experiment. Given that S is proportional to the deflection angle but inversely proportional to the square of the rotor–stator separation, decreasing the electrode separation d is a very effective way of increasing the angle responsivity of the instrument

Decreasing the rotor–stator separation is normally awkward because of the small distances involved. Limited by differential contraction on cool down, the closest the plates can be brought together when the magnetometer is set-up at room temperature while still allowing the magnetometer to work reliably when cooled to below 100 mK is $\sim 200 \mu\text{m}$. This corresponds to a rotor–stator capacitance of approximately 2.3 pF. We therefore devised a method for repositioning the stators when the magnetometer is cold.

In situ adjustment

Since we required a device that: was small enough to fit into the mixing chamber of the dilution unit; had a low heat dissipation in operation; and was relatively simple to use, piezo-electric actuation [13] seemed the best choice. However the rotor–stator separation of $200 \mu\text{m}$ is considerably larger than the range of movement afforded by a simple piezo-electric actuator, the change in length of a piezoceramic tube being given by

$$\Delta L = \frac{\beta LV}{W} \quad \{4\}$$

where L is the tube length, W its wall thickness, V the applied voltage and β a material dependent factor which is of the order 2 \AA V^{-1} at room temperature (and decreases by a factor of ~ 6 as the temperature is lowered to 4.2 K). To overcome this limitation, piezo-electric ‘stick-slip’ inertial drives were used [14].

The principle of operation of the inertial drive is as follows. A ‘puck’ is attached to two piezoceramic tubes (industry type PZT-5A in this case) [15] with a leaf spring, as shown in figure 2. If a voltage is applied to electrodes on a tube then it will lengthen, or contract (along the long axis in the figure). The spring tension is set such that the puck

will move with the PZT tube if it moves slowly but will slip if the tube is moved quickly. By applying a saw-tooth waveform the puck can be made to creep up, or down, the tubes.

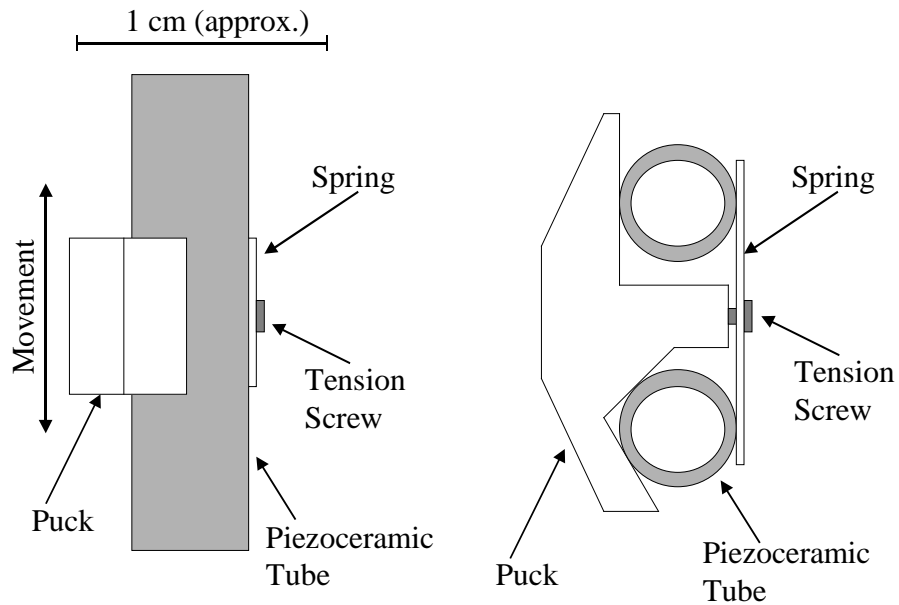


Figure 2. A sketch of one of the piezo-electric linear motors used in the experiment. An approximate scale is shown.

The instrument uses two of these stick-slip linear motors, modified from atomic force microscopy ‘coarse approach’ stages commercially available from Oxford Instruments [16], to enable the stators to be both translated and rotated so that the electrode separation can be minimised. A sketch of the actual magnetometer is shown in figure 3.

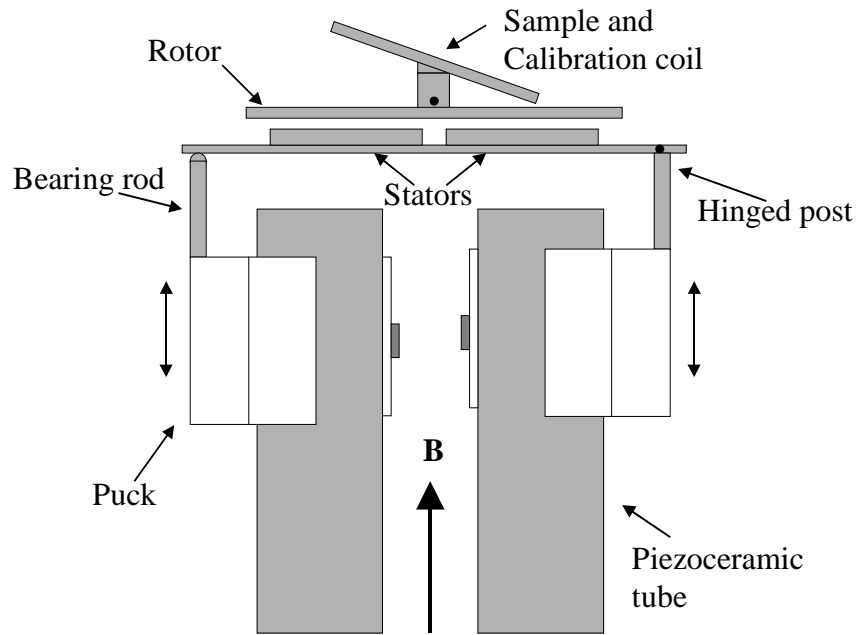


Figure 3. Diagram depicting the actual experimental arrangement looking along the axis of the torsion fibre. The experimental wiring and the grounding plate which surrounds the stators are not shown. Not to scale.

The pucks were machined from phosphor bronze, as were the bearing rod, hinged post and stators. Phosphor bronze was chosen for its low magnetostriction properties which we know from experience with previous magnetometer designs. The rest of the device, including the rotor, was machined from STYCAST 1266 epoxy [17].

Performance of the instrument

The initial testing of the magnetometer was performed in an Oxford Instruments AST200 dilution refrigerator [16] which has a base temperature of 8 mK and cooling power of $170 \mu\text{W}$ at 100 mK. The magnetometer was mounted in the mixing chamber of the fridge, below the phase boundary but in the ^3He circulation path. An adsorption pumped dilution unit is used as it has a low level of mechanical vibration during operation, since it dispenses with the need for large room-temperature pumps to circulate the ^3He .

The mixing chamber tail is accommodated inside the 52 mm bore of an Oxford Instruments superconducting solenoid capable of generating magnetic fields of up to 19 T

with a homogeneity better than 1 part in 10^3 over a 1 cm diameter spherical volume around field centre.

Equation {3} describes the measured signal, S , as a linear function of the rotor deflection and, as $\tau = k\phi$ where k is the torsion constant of the fibre, S should therefore be linear in the applied torque. This was tested using a phosphor bronze torsion ‘tape’ 30 mm long and $600 \times 25 \mu\text{m}$ in cross section. Figure 4 shows the relationship between torque and magnetometer output signal at a fixed field of 1 T, the torques were provided by passing known currents through an eight-turn coil, wound around a solid circular former 10 mm in diameter, attached to the sample support.

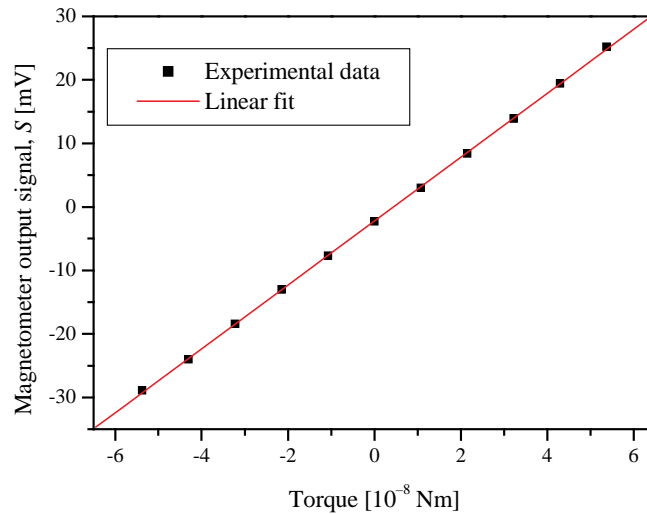


Figure 4. The relationship between the applied torque, at 1 T, and the magnetometer output signal. The plate separation d was $74 \mu\text{m}$ and the temperature was 30 mK. The bridge excitation was 10.6 V at 9531 Hz.

Equation {3} also predicts that the angle responsivity should scale as $1/d^2$ i.e. as the rotor–stator capacitance squared. This was confirmed by averaging the measured rotor–stator capacitance of each side of the magnetometer in order to find d , and then using a known change in torque, provided by the calibration coil, to measure the response of the instrument. The linear motors were then used to decrease the separation and the measurements were repeated. The results of this experiment are shown in Figure 5.

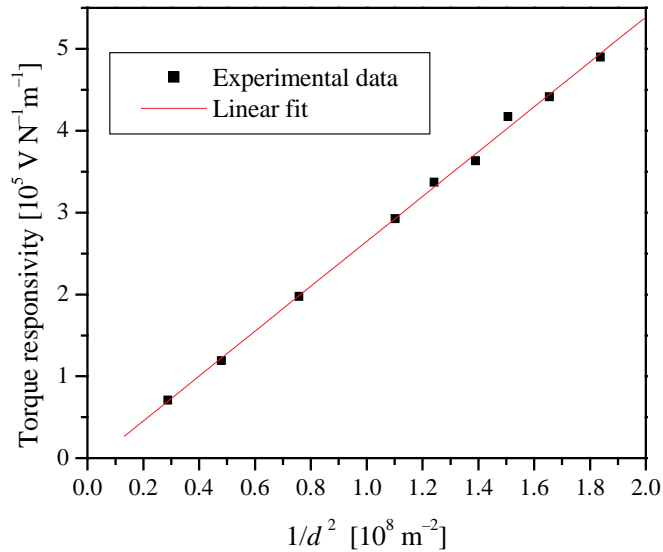


Figure 5. The relationship between the torque responsivity of the magnetometer and the rotor–stator separation. As expected the sensitivity is inversely proportional to the square of the electrode separation d . These data were obtained at a magnetic field of 1 T and a temperature of 30 mK.

Figure 5 also shows how well the piezo-electric linear motors worked. It was possible to adjust the rotor–stator capacitance to values greater than 6 pF in a matter of seconds, increasing the magnetometer responsivity by an order-of-magnitude compared with that which could be reliably achieved without them. The measured value of 6.3 pF corresponds to a rotor–stator separation of 74 μm , this is comparable with quoted values for the separation between the arms of micro-mechanical cantilevers and their ground plates [5].

Ultimate Sensitivity

Several figure-of-merit parameters are needed to describe the performance of a magnetometer. However, there is no universally adopted nomenclature, so in this section we shall briefly define and explain the terms we use in this paper.

The *responsivity* of the instrument is the ratio of a change in output signal to the size of a quasi-static stimulus giving rise to the change. The torque responsivity G_τ is

the quotient of the angle responsivity G_ϕ and the torsion constant k of the suspension fibre,

$$G_\tau = \frac{d\phi}{d\tau} G_\phi = \frac{1}{k} \frac{dS}{d\phi}. \quad \{5\}$$

The responsivity is the magnitude of the DC limit of the complex signal transfer function $G_\tau(j2\pi t)$ and the *signal bandwidth* and *equivalent noise bandwidth* are determined by the filter time-constant t of the lock-in amplifier

$$\Delta f_{\text{signal}} = 1/2\pi t \text{ and } \Delta f_{\text{noise}} = 1/8t \quad \{6\}$$

respectively for the 12dB/octave filter we use.

The *resolution* of an instrument is the smallest change in input stimulus distinguishable from noise. For a torque magnetometer, having an RMS output noise V_{noise} , and measurement bandwidth set by the lock-in time constant t as above, we consider that the torque τ_0 applied for a duration $t_0 \geq t$ is detectable when

$$(\tau_0 t_0)^2 \geq \frac{t_0 2\pi t V_{\text{noise}}^2}{G_\tau^2}. \quad \{7\}$$

This forms a basis for making a fair comparison between different magnetometer designs. To do this we define a smaller-is-better figure-of-merit, R , characterising the resolution

$$\min(\tau_0) = R\sqrt{t_0} \text{ where } R = \frac{V_{\text{noise}}\sqrt{2\pi t}}{G_\tau} \quad \{8\}$$

R , defined in this way, is independent of trivial changes to the instrument such as modifying the lock-in time-constant, or the signal-chain gain. However, R does reflect fundamental improvements, such as the elimination of a significant noise source.

It would be appropriate to quantify the *sensitivity* of an instrument by $1/R$. However, we avoid using this term because of the potential confusion which might arise from its common usage as a synonym for responsivity.

The resolution of the magnetometer is limited by noise and interference which can be of electrical or mechanical origin. We have attempted to minimise both sources in the current experimental design.

Mechanical noise

In order to reduce mechanical noise a vibration isolation system was built to support the experiment. The isolation system, similar to that described by Pickett [18], works by attaching the experiment to a large (secondary) mass which is supported, through a 4cm thick layer of Sorbothane [19] visco-elastic polymer, by another larger (base) mass which itself is floating on 4 Firestone model 29 airmount isolators [20]. The idea behind the two-stage construction is to provide effective high- and low-frequency isolation. All the pumping lines and cabling attached to the experiment are rigidly anchored to, or embedded in, the base block. The total mass supported by the airmounts is approximately 3×10^4 kg, and the whole structure is supported on its own foundations, separate from the rest of the building. This system is effective in reducing the mechanical noise transmitted to the experiment as can be seen by simply measuring the output signal of the magnetometer as a function of time using a short lock-in time constant, figure 6.

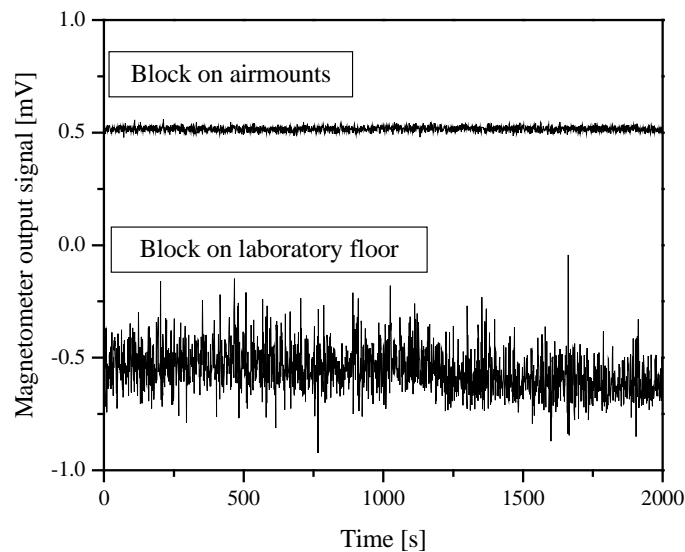


Figure 6. A comparison between the vibrational noise reaching the magnetometer with and without the air springs; the two traces are offset for clarity. The lock-in time constant was 20 ms with approximately one point taken per second. The improvement in the noise is apparent: the standard deviation of the data in the upper trace is a factor of $9.4 \times$ smaller than that in the lower trace.

Electronic noise

The sample orientation is detected by a differential capacitive displacement transducer [21] configured to maximise the responsivity with respect to angular rotations $\Delta\phi$ about the torsion fibre and minimise responsivity with respect to linear displacements of the suspension axis. The design of the electrode geometry, grounding, and shielding arrangements applied a methodology normally associated with ‘co-axial AC bridge’ systems [22]. In essence, this treats the grounding system as a network of finite impedances in its own right and explicitly considers the effects of ground currents and EMFs; this is in contrast to the more usual assumption of an equipotential grounding system. The benefit of this approach was a system that was immune to the usual causes of drift in such systems, *e.g.* changes in: cryogen level; cable positions; and contact resistance. The system could also have been upgraded, without major modification, to use a co-axial AC bridge, but experience showed this was not necessary.

Figure 1 is a schematic diagram. C_{1A} and C_{1B} represent the electrode structure on the sample rotor described above; rotating the sample increases/decreases C_{1A} as C_{1B} decreases/increases. The bridge is excited by a sine wave of amplitude ~ 10 V applied to the fixed electrodes and of frequency $f_0 \sim 10$ kHz. An isolated and accurately balanced differential excitation, provided by a magnetically shielded 1:1+1 audio isolation transformer X_1 , is needed for this circuit; this eliminates the effects of ground-loops and reduces the undesirable common-mode excitation level, a potential cause of troublesome ‘offset-null’ signals, to a negligible level. Two other contributions to the offset-null are: an in-phase component arising from slight changes in ϕ due to the stress caused by cooling; and a quadrature component due to wiring resistance and eddy-current losses. These were cancelled at the start of each run by adjusting a circuit represented by V_0 , C_0 and R_0 . The net induced charge at the common electrode of C_1 is proportional to rotation $\Delta\phi$ of the sample and this signal is first conditioned by the pre-amplifier on the top of the cryostat and then demodulated by an EG&G 5210 (or 7265) lock-in amplifier [23] at a safe distance from the magnet. The 15 V power supplies for the pre-amplifier are also provided by the lock-in.

Figure 7 shows the circuit in more detail. To achieve satisfactory practical performance with this type of circuit it is necessary to use high-quality components, and arrange all aspects of the wiring and grounding to preserve electro-mechanical symmetry. The offset-null circuit (R_0 – R_8 and C_0) is more complicated than implied by figure 1 because it must present a symmetric load to the isolation transformer and there must be range overlap between the polarities selected by $SW_{1,2}$.

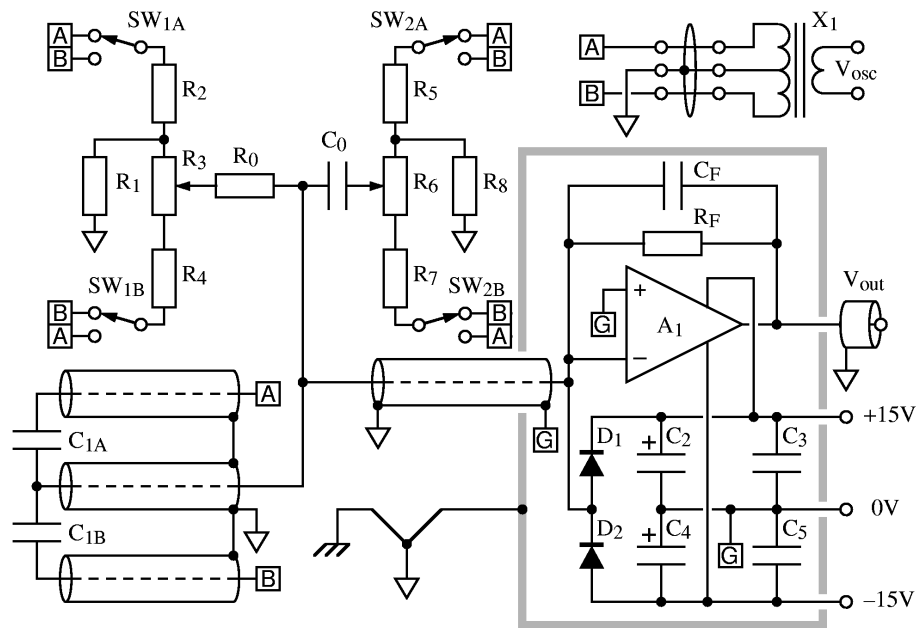


Figure 7. Circuit diagram of the bridge. Letters in squares represent connected nodes. Components are identified in Table 1. The coaxial cable between room temperature and the magnetometer (C_1) was Lakeshore type SS ultra-miniature co-ax cable.

The design could have been more elegant had suitable centre-tapped potentiometers been available at reasonable cost to use instead of $R_{1,3}$ and $R_{6,8}$ in which case the polarity switches would not have been necessary. The values of R_0 and C_0 are selected so that they have sufficiently high impedances not to impair the system responsivity. The pre-amplifier is enclosed in an electrostatic screen and shottky diodes ($D_1, 2$) protect it from accidental short circuits between the electrodes of C_1 . The operational amplifier A_1 and feedback components R_F and C_F were selected to permit operation up to *ca* 15kHz (figure 8a) and minimise the system noise (figure 8b) [24].

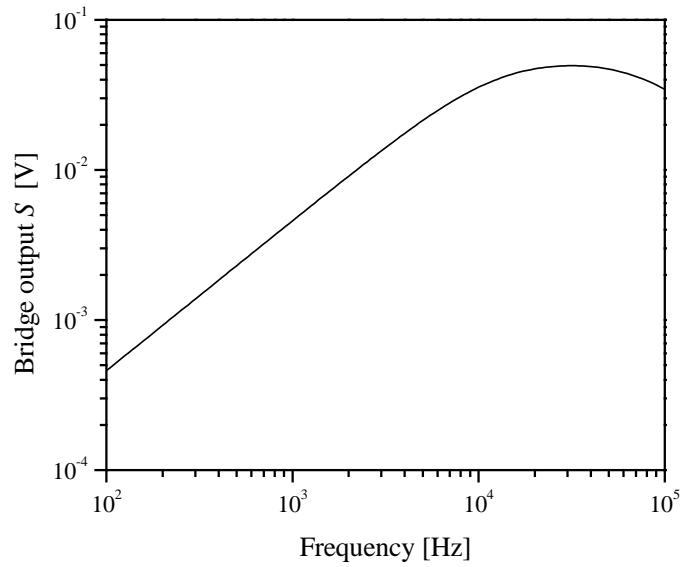


Figure 8a. Bridge output as a function of frequency (simulation). The curve shown is calculated using excitation voltage of 10 V and $C_{1a} = 6.36810$ pF, $C_{1b} = 6.29477$ pF. The coaxial cable between room temperature and the magnetometer (C_1) is 2 m (348 pF) in this example.

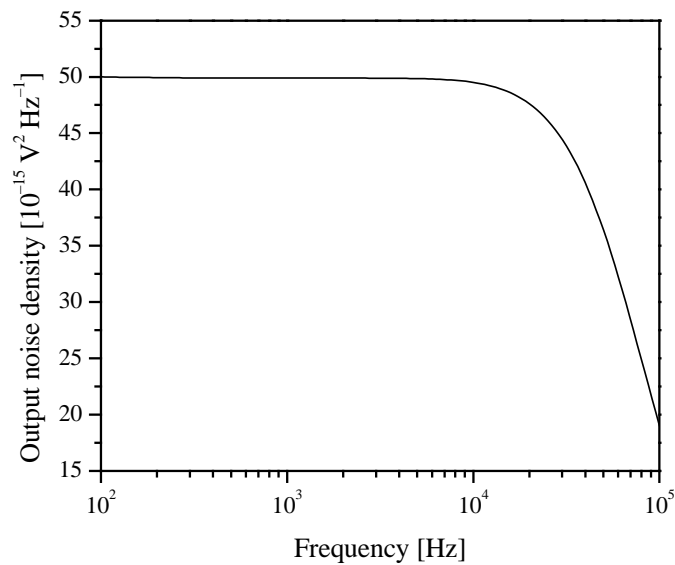


Figure 8b. Noise density spectrum at bridge output, (simulation).

We avoid frequencies above about 10kHz because relatively uncontrolled factors, such as cable – and other stray – capacitances, start to influence the responsivity and impair the medium term stability of the magnetometer.

Label in Figure 7	Component
R_0	500 k Ω metal film
$R_{1, 8}$	1 Ω wirewound
$R_{2, 4, 5, 7}$	100 k Ω wirewound
$R_{3, 6}$	100 Ω 10 turn, wirewound
A_1	AD743 (Analog Devices)
C_0	500 pF silver mica
$C_{2, 4}$	1 μ F tantalum
$C_{3, 5}$	0.1 μ F ceramic
$D_{1, 2}$	HP5082-2800 Schottky barrier
C_F	15 pF
R_F	1 M Ω metal film
X_1	1:1+1 audio transformer
$SW_{1, 2}$	DPDT gold plated contacts

Table 1. Parts list for figure 7.

This system has proved reliable and convenient in practice: the normal operating frequency (typically 10kHz) can be selected to minimise local sources of interference; the independent in-phase and quadrature offset adjustments mean that nulling the bridge is quick and accurate; and – most important from a practical point of view – the overall contribution of the bridge to the noise and drift of the magnetometer is negligible.

Absolute resolution

As mentioned in the introduction, in the literature there are reports of many magnetometers which quote a high angle-responsivity. However, in practice a more significant system parameter is the torque resolution. This is useful since it is torque that

is measured in the experiment and the size of this signal will depend on the applied field, sample carrier density and sample size (our magnetometer can easily accommodate samples with an area of 1 cm^2) as well as the torsion constant of the fibre.

Further testing of the magnetometer with a phosphor bronze torsion fibre with dimensions of 30 mm long by $250 \times 15 \text{ }\mu\text{m}$ has demonstrated torque responsivities of $G_\tau > 3 \text{ MV N}^{-1} \text{ m}^{-1}$. When the torque responsivity was $2.06 \text{ MV N}^{-1} \text{ m}^{-1}$ there was a noise level of $9.6 \text{ }\mu\text{V RMS}$ with a lock-in time constant of 300 ms, as in figure 9. This, applying {8}, is equivalent to a resolution of $6.5 \times 10^{-12} \text{ N m Hz}^{-\frac{1}{2}}$.

In experiments it is the resolution of the magnetometer, that is the smallest detectable signal, which is of interest. As shown, the resolution will depend on G_τ , the residual level of electro-mechanical noise and the measurement bandwidth. Since the equilibrium magnetization experiments can be performed quasi-statically a long lock-in time constant (3 – 10 s) can be used to reduce the effects of the residual electro-mechanical noise. This is not possible for the eddy current measurements as the magnetic field has to be swept relatively quickly (at rates of up to $\sim 20 \text{ mT s}^{-1}$) to obtain some of these data. However as the eddy currents are generally much larger than the dHvA signal (between 10 and 100 times) this is not a problem in practice.

Recently the performance of a magnetometer has been discussed in terms of the number of Bohr magnetons, μ_B , per electron that could be measured (for a sample with a given number density and at a given field). A value $\sim 5 \times 10^{-3} \mu_B$ was quoted by Schaapman *et al.* [7] at a base temperature of 1.2 K and with a measurement bandwidth of approximately 1 Hz [25]. In [7] the authors also compared their magnetometer to a cantilever design [5] which they claimed achieved a comparable figure.

Our design attains equivalent performance, and has the added advantage of facilitating experiments at much lower temperatures: down to 10 mK, two orders colder than [7] and over one order colder than [5].

Our facility for low temperature operation is important for the study of the physics of two-dimensional electron systems as it is at under these conditions that many-body effects, such as the fractional quantum Hall effect, begin to become important. To illustrate the practical application of our magnetometer, figure 9 shows data from an eddy current measurement on a high mobility 2DES sample (designated T477) grown at the University of Cambridge. After illumination when cold with red and infra-red light emitting diodes, the sample has a mobility of $510 \text{ m}^2 \text{ V}^{-1} \text{ s}^{-1}$ and a carrier density of $1.77 \times 10^{15} \text{ m}^{-2}$.

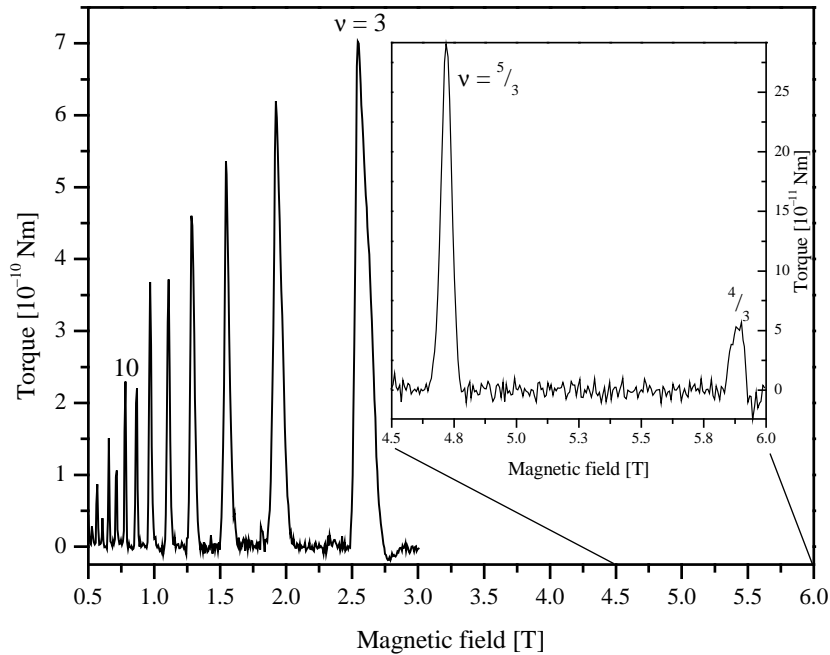


Figure 9. Induced currents, shown as their resultant torque, in sample T477 at 30 mK. Peaks are seen at both integer and fractional filling factors. A smooth background, which is roughly an order-of-magnitude larger than the eddy currents, has been subtracted from these data. The magnetic field sweep rate was approximately 8 mT s^{-1} , the lock-in time constant was 300 ms and one data point was recorded per second.

The data in figure 9 show induced currents at both integer and fraction filling factors. The small energy scale of the fractional quantum Hall effect energy gap [26] make these features strongly temperature dependent and highlights the advantages in the low temperatures attainable in these experiments.

Conclusion

We have developed a highly sensitive magnetometer for use at ultra-low temperatures. The device is robust and simple to use as the piezo-electric linear motors remove the need for precision alignment of the rotor and stators at room temperature. The vibration isolation system has proved effective in reducing the level of mechanical noise reaching the experiment and we have developed a stable, and highly sensitive, capacitance bridge with which the rotor deflections are measured. The magnetometer is capable of a resolution of $6.5 \times 10^{-12} \text{ N m Hz}^{-1/2}$. The attainable base temperature of the experiment is below 10 mK and this allows experiments to probe the fractional quantum Hall effect, even at filling factors greater than one.

Acknowledgements

The authors would like to acknowledge the contribution of Mr K White, whose exceptional workshop skills have been invaluable in the construction of our magnetometers. We are also grateful to Drs M Elliott and W G Herrenden-Harker of Cardiff University for many stimulating discussions on magnetometer design. This work was funded by HEFCE through the Joint Research Equipment Initiative (JR98EXUS), and by EPSRC through Grant number GR/R 37548.

References

1. Eisenstein J.P., Appl. Phys. Lett. **46** 695 (1985)
2. Templeton I.M., J. Appl. Phys. **64** 3570 (1988)
3. Potts A., Shepherd R., Herrenden-Harker W.G., Elliott M., Jones C.L., Usher A., Jones G.A.C., Ritchie D.A., Linfield E.H. and Grimshaw M., J. Phys. Condens. Matter **8** 5189 (1996)
4. Wiegers S.A.J., Specht M., Lévy L.P., Simmons M.Y., Ritchie D.A., Cavanna A., Etienne B., Martinez G. and Wyder P., Phys. Rev. Lett. **79** 3238 (1997)
5. Schwarz M.P., Grundler D., Meinel I., Heyn Ch. and Heitmann D., Appl. Phys. Lett. **76** 3564 (2000)

6. Harris J.G.E., Awschalom D.D., Maranowski K.D. and Gossard A.C., J. Appl. Phys. **87** 5102 (2000)
7. Schaapman M.R., Christianen P.C.M., Maan J.C., Reuter D. and Wieck A.D., Appl. Phys. Lett. **81** 1041 (2002)
8. Zhu M., Usher A., Matthews A.J., Potts A., Elliott M., Herrenden-Harker W.G., Ritchie D.A. and Simmons M.Y., Phys. Rev. B **67** 155329 (2003)
9. Eisenstein J.P., Störmer H.L., Narayanamurti V. and Gossard A.C., Superlattices and Microstr. **1** 11 (1985)
10. Jones C.L., Usher A., Cheng T.S. and Foxon C.T., Solid State Commun. **95** 409 (1995)
11. Watts J.P., Usher A., Matthews A.J., Zhu M., Elliott M., Herrenden-Harker W.G., Morris P.R., Simmons M.Y. and Ritchie D.A., Phys. Rev. Lett. **81** 4220 (1998)
12. Harris J.G.E., Awschalom D.D., Matsukura F., Ohno H., Maranowski K.D. and Gossard A.C., Appl. Phys. Lett. **75** 1140 (1999)
13. For a review, see Hemsell T. and Wallaschek J., Ultrasonics **38** 37 (2000)
14. Pohl D.W., Rev. Sci. Instrum. **58** 54 (1986)
15. Staveley NDT Technologies, Kennewick, USA <<http://www.staveleyndt.com>>
16. Oxford Instruments PLC, Oxford, UK <<http://www.oxinst.com>>
17. Emerson and Cuming, Billerica, USA <<http://www.emersoncuming.com>>
18. Pickett G.R., Rep. Prog. Phys. **51** 1295 (1988)
19. Sorbothane Incorporated, Kent, USA <<http://www.sorbothane.com>>
20. Firestone Industrial Products Company, Carmel, USA <<http://www.fsipweb.com>>
21. Hugill A.L., J. Phys. E: Sci. Instrum. **15** 597 (1982)
22. Kibble B.P. and Rayner B.H., *Coaxial AC Bridges* (Institute of Physics Publishing, Bristol, 1984)
23. Advanced Measurement Technology, Inc. Oak ridge, USA
<<http://www.signalrecovery.com/5210.htm>>, <<http://www.signalrecovery.com/7265.htm>>
24. Williams C.D.H., 'MacSpice 3f5' version R6 (2003)
<<http://newton.ex.ac.uk/teaching/CDHW/MacSpice/>>
25. Schaapman M.R, private communication.

26. For a review, see Chakraborty T. and Pietiläinen P., *The Fractional Quantum Hall Effect* (Springer-Verlag, Berlin, 1988)